ACS APPLIED MATERIALS & INTERFACES

Research Article

www.acsami.org

Biomolecular Gradients via Semiconductor Gradients: Characterization of Amino Acid Adsorption to $In_xGa_{1-x}N$ Surfaces

Lauren E Bain,[†] Scott A Jewett,[‡,§] Aadhithya Hosalli Mukund,[⊥] Salah M Bedair,[⊥] Tania M Paskova,[⊥,#] and Albena Ivanisevic*[,†,#]

[†]UNC/NCSU Joint Department of Biomedical Engineering, [⊥]Department of Electrical and Computer Engineering, and [#]Department of Materials Science and Engineering, North Carolina State University, Raleigh, North Carolina 27606, United States

[‡]Weldon School of Biomedical Engineering, Purdue University, West Lafayette, Indiana 47907, United States

Supporting Information

ABSTRACT: The band gap of indium gallium nitride can be tuned by varying the compositional ratio of indium to gallium, spanning the entire visible region and extending into the near-infrared and near-ultraviolet. This tunability allows for device optimization specific to different applications, including as a biosensor or platform for studying biological interactions. However, these rely on chemically dependent interactions between the device surface and the biostructures of interest. This study presents a material gradient of changing In:Ga composition and the subsequent evaluation of amino acid adsorption to this surface. Arginine is adsorbed to the surface in conditions both above and below the isoelectric point, providing insight to the role of electrostatic interactions in interface formation. These electrostatics are the driving force of the observed adsorption behaviors, with protonated amino acid demonstrating increased adsorption as a function of native surface oxide buildup. We thus present a gradient inorganic substrate featuring varying affinity for amino acid adhesion, which can be applied in generating gradient architectures for biosensors and studying cellular behaviors without application of specialized patterning processes.

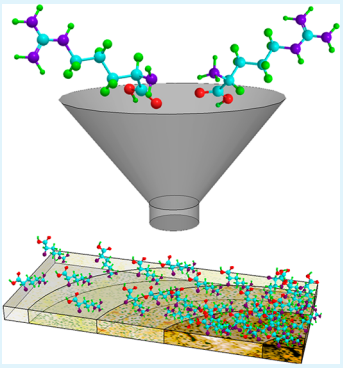

KEYWORDS: *III−V semiconductor, indium gallium nitride, X-ray photoelectron spectroscopy, surface gradient, amino acid, atomic force microscopy*

1. INTRODUCTION

Group III-nitride materials emerged as promising candidates for producing blue-green LEDs in the early 1990s, exhibiting markedly increased efficiencies and intensities when compared with the existing SiC-based technologies.[1] As these materials were characterized and growth methods improved, they began drawing attention for the unique optical and electronic properties, including their wide band gap and electron transport characteristics.[2−4] The specific ternary combination of $In_xGa_{1-x}N$ features tunability from the near-IR to the near-UV, spanning the entirety of the visible spectrum and offering unique physical and chemical characteristics for different ratios of In to Ga.[5] InGaN also presents the opportunity to create an improved chemical sensor or biosensor by combining the advantageous properties of GaN, including chemical stability[6] and biocompatibility,[7,8] with those of InN, including a high surface electron concentration.[3,4,9]

Light-emitting diodes present a unique platform for optical detection of chemical analytes. Interactions at the inorganic surface alter the surface-state structure of the material, changing the electroluminescence and providing a measurable indication of analyte binding at the surface.[10−12] GaN has also been used to create field effect transistor-based sensors, where interactions at the gate surface modulate the conductivity of the underlying substrate, again generating a measurable signal attributed to surface interactions.[13−15] In both cases, providing specificity to a given analyte relies on manipulating the surface interactions that take place on the material, often by modifying the chemical species present at the surface. Further increase the electrical response of the GaN-based FET architectures can be achieved by increasing surface sensitivity through incorporation of InN and considering near-surface component of InGaN or InN, the latter known by its electron accumulation layer at the surface.[9]

Bioinorganic interfaces have been discussed and researched extensively over the past 20 years. By coupling the electrical properties of semiconductors with the biological specificity and variety of proteins and biomolecules, novel devices for probing nanoscale interactions and integrating digital electronics with biological systems can be developed.[16] Creating an interface between the semiconductor substrate and the desired biomolecule has produced a surge in studies documenting novel functionalization schemes. The literature is rich with resources on surface modification of GaN, including photochemical patterning with alkenes[17] and direct functionalization by exposure to a glow discharge plasma and humidified air.[18] Multiple efforts have been devoted to patterning surfaces with

Received: April 29, 2013
Accepted: July 10, 2013
Published: July 10, 2013

spatially specific chemistry,[19,20] viscoelastic properties,[21] surface energy,[22] and morphological features.[23] These processes offer applications in studying cellular responses to different stimuli, with cell membrane proteins responding to the surface patterning—be it chemical, morphological, or mechanical—and triggering different phenotypic behavior. Developing surface gradients for cell studies expands this evaluation, increasing the extent to which the extracellular environment can be precisely tuned.

Surface modification of a substrate depends on multiple properties of the underlying material, including the topographic features and chemical species involved in the generated interface. This has been illustrated by mapping amino acid adhesion to a range of materials, including insulators, metals, and a selection of semiconductors,[24] as well as phage display experiments on Si,[25] InN,[9] GaN,[26] and GaAs.[25] Within the GaAs samples, the recognition peptide featuring the strongest adhesion varies based on crystal orientation presented, providing more evidence for the high degree of specificity encountered with these phage screenings.[25] The origins of this surface-specific binding have also been modeled in a single-molecule system, demonstrating the influence of even a single amino acid mutation on the strength of interaction.[27] As such, we present a novel surface for use in generating molecular gradients, Figure 1. Rather than relying on complex surface functionalization tactics, a surface gradient is introduced during material growth. This semiconductor gradient can be exposed to an adsorbate in solution and will exhibit variable surface adhesion and coverage based on compositional changes. A demonstration of this preferential affinity is performed using a single amino acid, highlighting the role of surface chemical variations in bioinorganic interface formation.

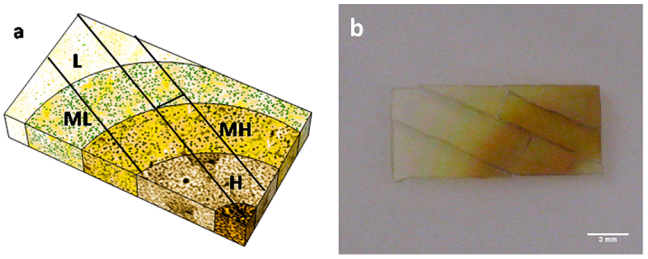

Figure 1. (a) Schematic and (b) photograph of the In_xGa_{1-x} substrate. (a) Regions corresponding to In:Ga are indicated by color, whereas bold black lines indicate substrate dicing. The regional designations indicate High In:Ga (H), Mid-High In:Ga (MH), Mid-Low In:Ga (ML), and Low In:Ga (L). (b) Photograph and scale of the diced sample. Full substrate dimensions are 15 mm × 6 mm. Scale bar 3 mm.

2. EXPERIMENTAL SECTION

$In_xGa_{1-x}N$ Growth. A thin $In_xGa_{1-x}N$ film was grown by metal organic chemical vapor deposition (MOCVD) on a sapphire substrate. Conventional growth at 350 mTorr was performed using a low-temperature GaN buffer layer of about 100 nm thickness grown at 475 °C. Trimethylgallium (TMGa) and trimethylindium (TMIn) were used as III-group sources. A few components of the MOCVD reactor were custom designed to enable the specific goals of this growth experiment. The quartz tube that brings reaction components to the growth surface features an additional quartz plate along the length of the tube, dividing the volume into two columns to enable separate introduction of the NH_3 flux and III-group source. This also enables a possibility for one-column mode for asymmetric, noncentered introduction of all the fluxes. The sample holder allows off-center positioning, again facilitating the creation of nonsymmetric surfaces. Although rotation is typically utilized to ensure uniform growth and was used to generate the underlying buffer layer growth, rotation was stopped for growth of the upper layer to ensure radial nonuniformity across the sample surface.

The nonuniformity in the In composition is due to the lack of uniformity of both the growth rate and the absolute TMIn flux impinging on the surface. We had previously shown that In incorporation in the solid phase depends both on the residence time and the desorption rate of the In atoms on the growing surfaces.[28,29] High growth rate traps the In atoms in the growing surface before their desorption, resulting in high In amount in the solid phase. The same arguments can be used with high TMIn flux at the growing surfaces. Having all gases coming from the same channel with relatively small dimension increase the fluxes for both In and Ga precursors leading to a higher growth rate and a higher TMIn fluxes at the growing surface. The lack of uniformity in the TEGa and TMIn is due to the off-centered channel axis and the off centered wafer disposition. Thus, the group-III fluxes are very high on one side of the substrate, the one closer to the channel axes, and relatively lower on the other side of the stationary substrate. Even though the In/Ga flux ration is the same all over the substrate, the absolute In flux is not uniform, resulting in a nonuniform In incorporation in the solid phase.

All data were collected on representative sample with as grown size of 14 mm × 14 mm sample. The sample was diced in multiple small pieces and every sample was treated at identical conditions and special care was taken to ensure characterization under identical conditions. The film thickness is of about 1.5 μm. The thickness nonuniformity across the surface of the representative sample described here is of about 20%. The layer thickness of the $In_xGa_{1-x}N$ layers grown in the MOCVD reactor can be varied in the range of 1.0−2.8 μm. The surface morphology of the MOCVD-GaN layers with thickness in that range, grown at identical conditions, is consistently and reproducibly very similar. These considerations make us believe that a possible thickness variation across the sample surface does not contribute to the surface property variation described.

Photoluminescence Measurements. Photoluminescence (PL) measurements were carried out at room temperature with 325 nm excitation from a continuous wave He−Cd laser. The spectra were recorded with a 0.5 m monochromator, photomultiplier tube, and standard lock-in amplifier technique in the 350−650 nm spectral range.

Atomic Force Microscopy. Data were collected using the Asylum Research Cypher scanning probe microscope (Santa Barbara, CA) with Asylum silicon nitride probes (Model TR800PSA.) Samples were mounted on carbon AFM pucks using nonwater-soluble Crystalbond 509−3 (Ted Pella, Redding, CA) to avoid dissolution and deposition of adhesive on sample surfaces during imaging. Imaging was carried out in pH-adjusted PBS solution using 200−250 μL solution placed on the sample to avoid droplet effects. Topography images (5 × 5 μm^2) were collected at representative points for each region of the substrate. Topography images were acquired at the beginning and end of each adhesion force collection to verify the stability of surface features. Root-mean-squared (RMS) roughness, a value that describes the standard deviation in height for a given sample area, was calculated using the *Igor Pro* software. Force curve acquisition was carried out under the same solution conditions, with 300 force curves acquired for each region of the substrate. Analysis of adhesion forces and depth profiles was performed using *Igor Pro* software. For determining defect depth and radius, 20 defect pits were selected within each topographic region. Force mapping was performed using a 32 × 32 pixel map for a 1 × 1 μm^2 area. Following analysis, data were exported to Matlab (version R2011b) for visualization.

X-ray Photoelectron Spectroscopy. A Kratos Analytical Axis Ultra X-ray photoelectron spectrometer with a monochromated Al Kα source was used to acquire XPS data. High resolution spectra of Ga 2p and 3d, O 1s, C 1s, N 1s, In 3d, and S 2p were collected at 0° photoemission angle with 20 eV pass energy. Survey scans (0−1200 eV) were collected at 0° photoemission angle with 160 eV pass energy. Data analysis and peak fitting was performed using CasaXPS software,

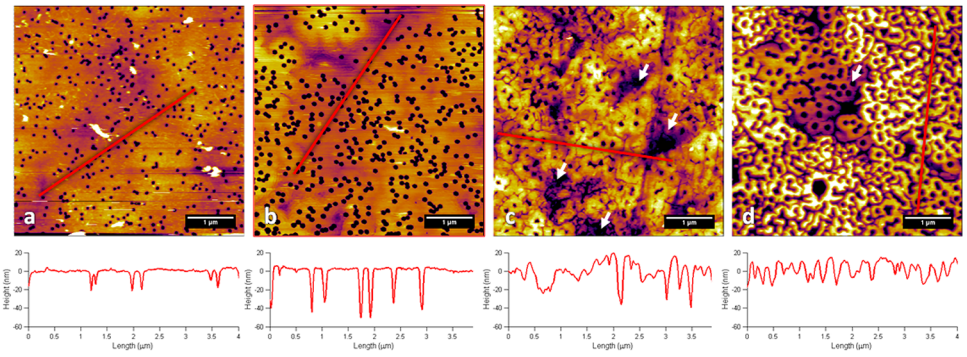

Figure 2. Topographic variations in InGaN as a function of In:Ga (a–d represent L–H, respectively.) Crystallographic pit defects increase in size and decrease in density with a decrease in Ga composition, and micrometer-scale variations (shadowed regions in c and d, indicated by white arrows) emerge. Line scans (indicated by red lines) provide depth profiles of the surfaces and defects. Scale bars are 1 μm.

version 2.3.16. Charge shift was calibrated to the adventitious carbon peak of the C 1s spectra (284.8 eV.) Peak fitting was performed using a summed Gaussian and Lorentzian shape with a subtracted Shirley background. The presented spectra were normalized prior to plotting. Data were normalized and plotted using Matlab (Version R2011b.)

Surface Preparation. The $In_xGa_{1-x}N$ sample was cleaved into several sections using a diamond scribe, as shown in Figure 1, generating three sets of samples with varying In:Ga ratios: one set for AFM experiments, one set for XPS, and one set used for both experimental procedures to further confirm any observed trends. Between experiments, sections were solvent cleaned by sonication for 5 min each in acetone, ethanol, and deionized water. Following experiments involving incubation in arginine solution or PBS, samples were soaked for 10 min in 80 °C deionized water to assist in salt removal from the surface. Prior to either arginine incubation or experiments on cleaned surfaces, a 10 min etch in 37% HCl was used to further clean the surfaces and remove any significant surface oxide buildup. This etch is not expected to completely eliminate and prevent surface oxide formation; rather, it is a secondary step to assist in the removal of contaminants from the surface. Following exposure to HCl, samples are rinsed three times in deionized water and dried with N_2. 0.01 M PBS buffer consisted of one PBS tablet (Fisher, BP2944–100) dissolved in 200 mL of deionized water. pH adjustment was performed using 1 N HCl and 1 N NaOH. This pH-adjusted PBS is also used to maintain solution conditions during AFM experiments. Arginine solution was prepared by dissolving powdered L-arginine in pH-adjusted PBS for a final arginine concentration of 1 mM. Samples were immersed in arginine solution overnight (~16 h.) Prior to analysis, samples were dried with N_2 gas.

3. RESULTS AND DISCUSSION

To date, the standard approach to generating surface gradients involves using either microfluidic[30,31] or photochemical[32−34] processes to introduce surface features on a uniform substrate. Preparation of chemically defined substrates during semiconductor growth creates the possibility of gradient fabrication without these additional procedures, utilizing the affinity of biomolecules for specific surfaces as a selective functionalization scheme.[25]

3.1. Characterization of $In_xGa_{1-x}N$ Gradient. $In_xGa_{1-x}N$ gradient materials feature unique optical properties in accordance with the variation in the In composition, x, as represented by the illustration in Figure 1. Higher-In-composition regions are significantly darker and more opaque, whereas a reduction in In results in a lighter color with greater transparency. To maintain experimental consistency, this gradient has been divided into regions delineated by the black lines and blocks of color in as shown in Figure 1.

The variation of In:Ga ratio across the sample surface was confirmed by the shift of the emission band in the PL spectra recorded in four different regions of the $In_xGa_{1-x}N$ sample (Supporting Information, Figure S0). we used the In composition relation with the band gap energy in the $In_xGa_{1-x}N$ alloys with a clear bowing shape previously found consistent with experimental data[35]

$$E_g^{InGan}(x) = xE_g^{InN} + (1 - x)E_g^{Gan} + bx(1 - x) \quad (1)$$

where b is the bowing parameter of 1.51.[35] We calculated the In composition in the different spots to vary from 29.2 to 31.1%. Independent measurements performed by X-ray diffraction confirmed the variation of In composition again manifested by a shift of the peak position (not shown here) in the $2\theta-\omega$ scans of 002 reflection.

Variations in surface topography emerge when studying the surface gradient using AFM, as shown in Figure 2. Region L exhibits smaller, shallower defect pits of high density over the underlying terrace structure common to GaN. As In:Ga ratio increases, the density of these pits changes, as does the depth and overall consistency of the underlying structure. The overall hexagonal shape of the defects is indicative of the underlying wurtzite crystalline structure characteristic of both GaN and InN. The different size of the pits can be attributed to threading dislocations of different type in the crystal lattice.[36,37] Micron-scale variations in topography emerge, contributing to the RMS values provided in Table 1. RMS roughness increases for the intermediate regions of the substrate, and the general variability can be attributed to the changing defect morphology as well as composition variations in the underlying InGaN substrate. A representative line scan of the defect profiles in each region is also provided in Figure 2. Depth profile data for the defects,

Table 1. RMS, Defect Depth, and Defect Width Values[a]

	L	ML	MH	H
RMS (nm)	4.7	11.5	11.6	9.4
defect depth (nm)	18 ± 2	54 ± 9	48 ± 8	24 ± 2
defect width (nm)	120 ± 10	140 ± 10	140 ± 30	150 ± 20

[a]Variations in pit size and density, as well as general micrometer-scale topographic changes, yield a variation in RMS roughness across the substrate. Depth and width values include the standard deviation from 20 defect pits. Although the defect width is fairly consistent across the substrate, there is a more significant variation in the defect depth.

given in Table 1, reveals that the defect depth varies significantly across the substrate.

Although the literature is rich with studies featuring optical characterization of $In_xGa_{1-x}N$ systems[38−40] there are fewer resources devoted to analysis of the surface chemical effects that become apparent when scanning across a surface gradient. Thus, it is of interest to acknowledge several features of the XP spectra that emerge due to the changes in Ga−N and In−N bonds as the ratio of In to Ga changes. As displayed in Figure 3,

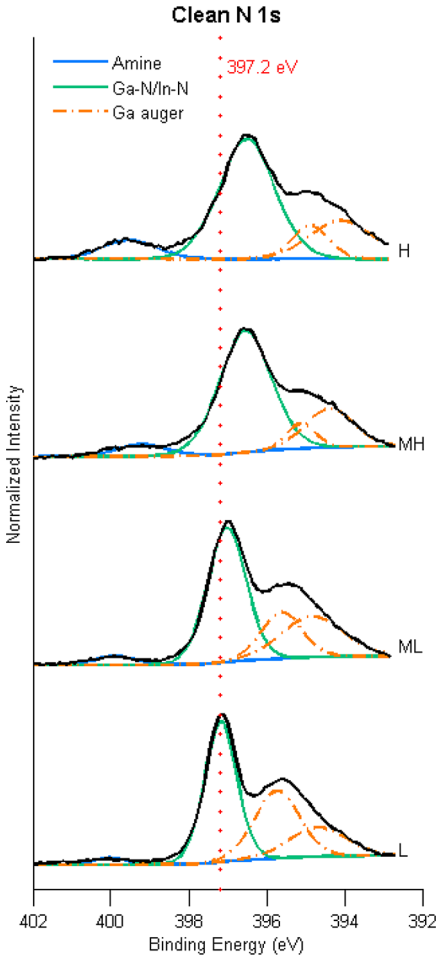

Figure 3. Peak shift in the N 1s spectra. The 397.2 eV center of the region L spectrum is indicated by the red dotted line, illustrating a shift to lower binding energies concomitant with an increase in In:Ga.

there is a shift in the energy of the peak attributed to Ga−N/In-N bonds in the N 1s spectra when moving to regions of higher In:Ga. This shift to lower binding energies is due to the decreased electronegativity of In when compared to Ga, causing a drop in the binding energy between the group III material and nitrogen. The Ga 3d spectrum, seen in Figure 4, features the emergence of a secondary doublet attributed to In 4d[41] in addition to the primary Ga 3d doublet.[42] These overlapping doublets provide a qualitative assessment of the ratio of In to Ga at the surface.

3.2. Adsorption Behavior of L-Arginine. A compelling case for investigating surface modifications, particularly the generation of surface gradients, can be made when considering applications in cellular biology. Cells are well-known to respond to gradients of biomolecular cues; one specific example is the recruitment of neutrophils and macrophages from the vasculature to damaged tissue. The chemical gradient generated by diffusion of the products of tissue inflammation guides the migration of these responsive white blood cells to the wound site.[43] Characterizing cellular responses to differentially patterned growth cues is critical to better understand how the extracellular microenvironment dictates physiological processes. Many platforms have been developed to assess the influence of gradient cues on cellular behaviors;[44] however, fabrication techniques for generating these surface gradients remain complicated, adding multiple steps to standard surface preparation procedures. By demonstrating differential adsorption behavior of a biomolecule across a gradient material, we hope to illustrate the potential of these substrate compositional gradients as a method of fabricating biomolecular interfaces without these additional preparation steps.

The physiological environment in which cells grow and develop features a myriad of enzymes, hormones, and proteins, all of which play different roles in dictating cellular phenotypes and responses. These cues are often large molecules with complex interactions taking place both within the molecule and with the surrounding environment. It is thus standard[16] and advantageous to use a comparatively small, simple biomolecule (e.g., L-arginine) for characterizing interface formation prior to investigating complex proteins or polypeptides. The extent to which the underlying gradient is maintained by differential physisorption of arginine is confirmed using both AFM and XPS, as demonstrated below.

The L-arginine preparation conditions were selected based on the pK_a of the α-amine group. The protonation point for this α-amine is pH 9; therefore, the arginine population is largely protonated at the pH 6 condition, whereas pH 12 features the deprotonated α-amine. These charged groups dictate how polar interactions take place between individual amino acid molecules and will play a significant role in the adsorption behavior on the $In_xGa_{1-x}N$ gradient. Figure 5 demonstrates a representative topography image of adsorbed amino acid in the protonated state. The surface features remain stable over the 30 min time course of the AFM experiments. This follows arginine exposure, substrate drying, and introduction of PBS for AFM measurements. Electrostatic repulsion due to the positive charges on both the α-amine and the guanidium cap contributes to the formation of distinct clusters across the surface, while the defect pits remain visible. Cluster formation has been observed previously,[27,45] and is attributed to interactions between the side chains and the underlying substrate. This behavior is also observed to some extent in the nonprotonated state with an increased surface presence of amino acid, represented by the increased cluster density (see the Supporting Information, Figure S1.) The extent to which the underlying topographic variations influence surface adsorption, as opposed to chemical or electrostatic contributions to cluster formation, is an important concept that may play a role in reusability of devices or general approaches to chemical functionalization. A recent study investigated two chemical functionalizations of nanotextured GaN, finding a variation in contact angle dependent on both texture and functionalization process.[46] As such, future modeling studies isolating topographic effects from the other forces dictating biomolecule adsorption on a gradient will contribute to understanding the dynamics of interface formation.

Measuring the force of adhesion of biomolecules to a substrate is a common technique used to assess the mechanical properties of the biosubstrate interface.[47] An adhesive

dx.doi.org/10.1021/am4015555 | ACS Appl. Mater. Interfaces 2013, 5, 7236−7243

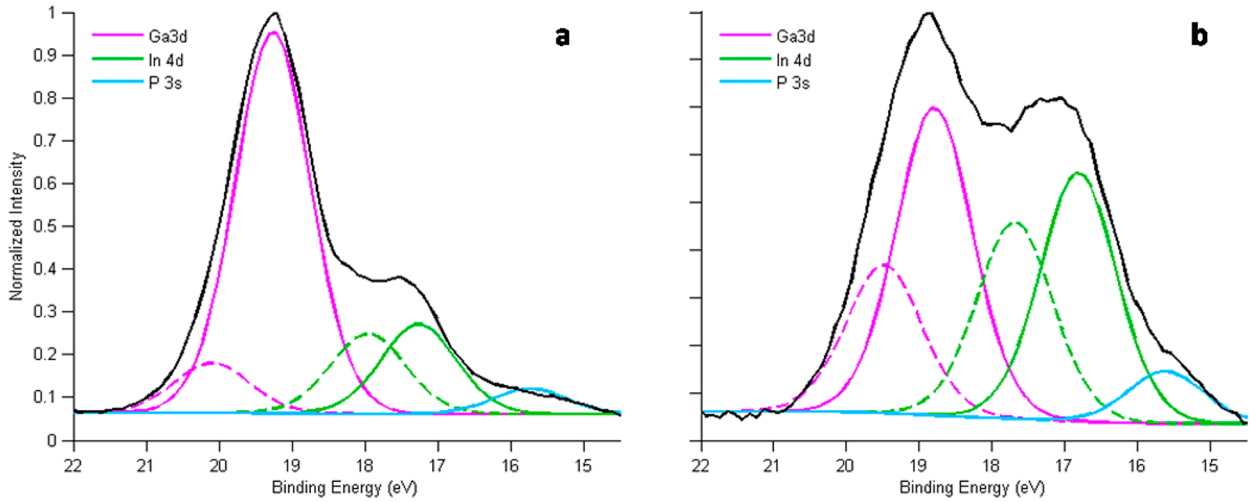

Figure 4. Ga 3d XP spectra of region (a) ML and (b) MH. The spectra feature two doublets, Ga 3d and In 4d, with a small phosphorus peak attributed to the PBS used during sample preparation. As expected, the relative contribution of In 4d to the overall shape increases with increasing In:Ga.

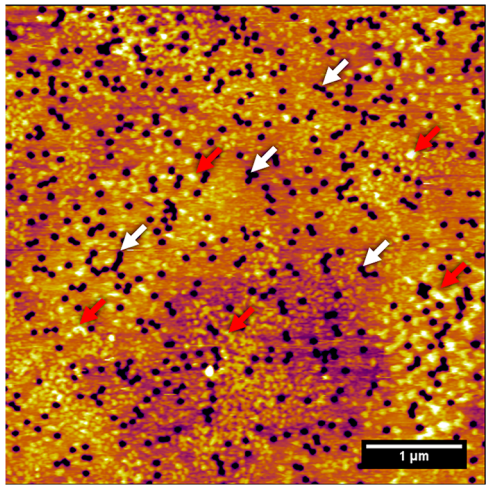

Figure 5. Clusters of amino acid on the low In:Ga surface, observed following incubation of surfaces in L-arginine at pH 6. A small selection of defect pits and amino acid clusters are indicated by white and red arrows, respectively.

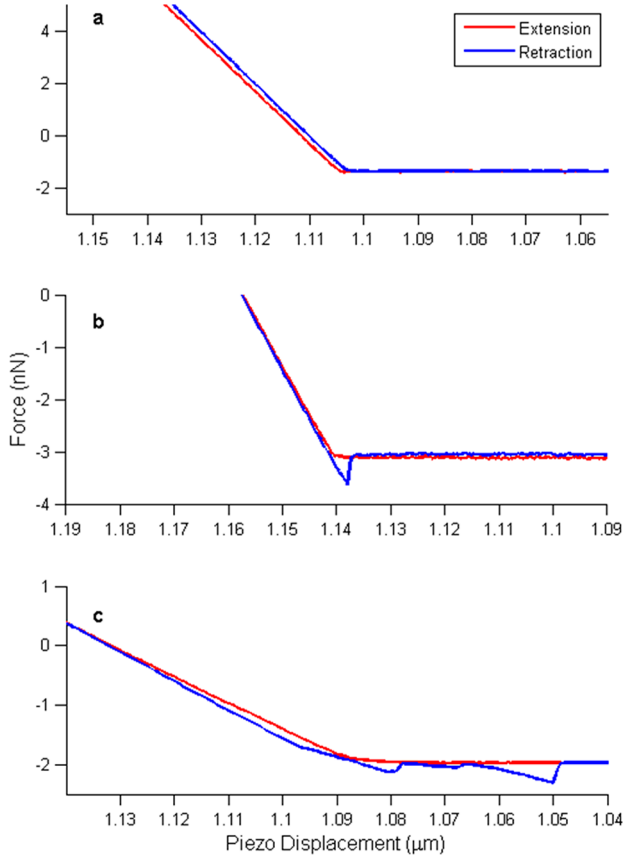

Figure 6. Representative force–distance curves, indicating the three characteristic adhesion shapes. (a) No significant interaction presents overlapping extension and retraction. (b) A single adhesive event is seen in the added force in the retraction curve at the point of departure from the surface. (c) Multiple adhesive events are represented by the multiple local extrema in the retraction curve.

interaction takes place between the AFM tip and the surface biomolecule, allowing the strength of the attachment between biomolecule and substrate to be assessed as the tip withdraws from the interface. Figure 6 depicts three characteristic force–distance curve shapes observed when acquiring adhesion data: No adhesion to the surface,[47] seen in Figure 6a; one adhesive event,[47] seen in Figure 6b; and multiple adhesive events, which has previously been attributed to conformational changes[48] and is observed in Figure 6c. Although all force curves collected featured these curve shapes, there was significant variation for curves acquired at a single point. Table 2 provides the adhesion data, demonstrating the magnitude of this variation (on the order of the average adhesion force calculated). Representative histograms of the data are provided in the Supporting Information (Figure S2). This high variance is attributed to the observed variation in substrate topography; as discussed in Figure 5(clusters), the presence of discrete clusters of peptide yields different adhesive behavior "on" vs "off" one of these clusters, as can be illustrated by force-mapping a given substrate region (see Supporting Information, Figure S3.) This large standard deviation is largely indicative of localized inconsistencies in arginine accumulation, confirmed by the appearance of clusters in the topography images.

dx.doi.org/10.1021/am4015555 | ACS Appl. Mater. Interfaces 2013, 5, 7236–7243

Table 2. Summary of Adhesion Data Extracted from AFM Force Curves

	cleaned surface				pH 6 L-arginine				pH 12 L-arginine			
	L	ML	MH	H	L	ML	MH	H	L	ML	MH	H
adhesion force (pN)	273	142	196	373	264	419	649	346	126	55	270	323
SD (pN)	207	224	255	420	229	304	637	324	229	133	385	391

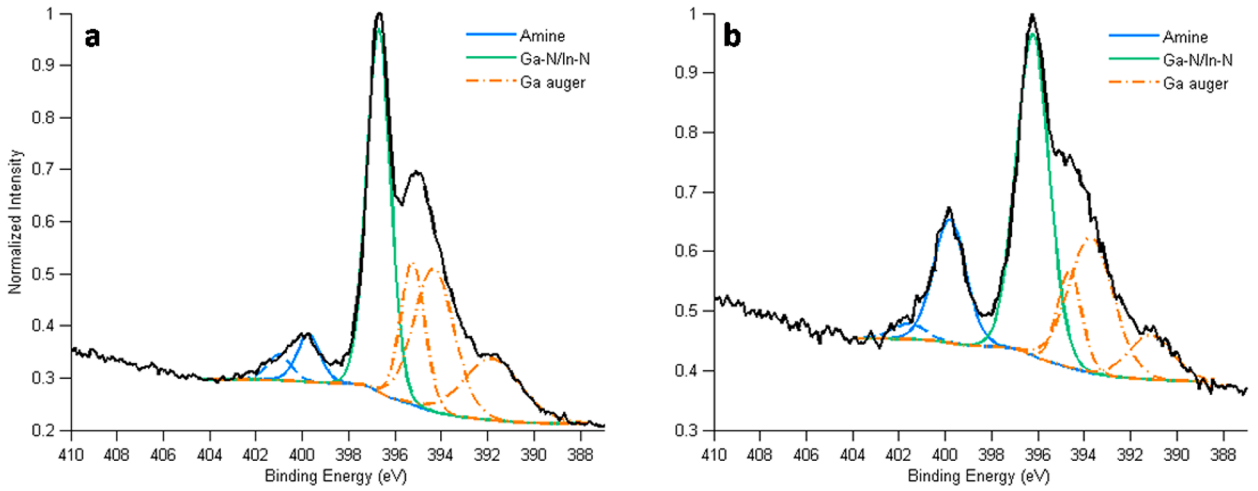

Figure 7. Representative increase in the amine (NH_2/NH_3^+) contribution to the N 1s spectra with an increase in In:Ga. Region (a) ML and (b) MH.

Table 3. Summary of Chemical Data Acquired via XPS[a]

		cleaned				pH 6 L-arginine			
		H	MH	ML	L	H	MH	ML	L
surface at %	C	44.7	39.2	29.8	26.4	37.2	30.3	21.5	28.5
	Ga	18.1	22.5	29.6	45.0	12.5	8.4	23.4	30.0
	In	6.7	7.5	7.1	2.4	6.8	5.0	4.3	4.0
	N	21.1	21.2	23.0	17..5	16.9	14.3	17.8	15.2
	O	9.4	9.6	10.6	8.7	26.5	42.1	33.0	22.3
oxide (% of peak)	Ga 2p	4.8	4.7	5.2	5.6	2.8	4.7	5.88	6.9
	In 3d	19.3	18.2	5.6	8.2	22.0	15.6	6.70	5.6
ratio to Ga 3d	In	0.37	0.33	0.24	0.05	0.55	0.60	0.18	0.13
	O	0.52	0.43	0.36	0.19	2.11	5.03	1.41	0.74
	C	2.47	1.74	1.01	0.59	2.97	3.62	0.92	0.95
	NH_2/NH_3^+	0.11	0.06	0.03	0.01	0.11	0.31	0.06	0.03

[a]The low binding energy of the Ga 3d spectra yields minimal attenuation due to surface effects, providing a stronger assessment of the surface chemistries involved in a given surface.

In addition to the formation of clusters of arginine on the surface, the N 1s XP spectra for the pH 6 case illustrates the emergence of a more significant amine peak, as can be seen in Figure 7. This is attributed to the NH_2/NH_3^+ groups present on the L-arginine molecule. The pH 12 spectra (Supporting Information, Figure S4) illustrate a distinct amine peak with no Ga auger or In−N/Ga-N peaks. For all substrate regions, there is complete occlusion of the Ga and In signatures, indicating formation of a surface multilayer large enough to completely occlude the underlying substrate. After a simple rinse step, the In and Ga signatures reemerge, suggesting that a simple water rinse is capable of removing some amount of the surface bound arginine. The emergent In and Ga peaks are more significant for the low In:Ga regions, again suggesting that the interface between arginine and the high-In substrate regions demonstrates improved stability.

3.3. Inorganic vs Organic Gradient on $In_xGa_{1-x}N$. A summary of the collected chemical data for both the inorganic gradient surface and the subsequent amino acid-treated surface is displayed in Table 3. The surface ratios to Ga 3d provide a useful description of surface chemistry, as the Ga 3d spectrum features low binding energy peaks and, as such, minimal attenuation due to irregularities at the surface. For the cleaned surfaces, the surface ratio of In:Ga does decrease from region H to region L. This accompanies a decrease in surface oxide, suggesting that the high-In regions oxidize more readily than the low-In regions. A similar decrease in surface oxide is observed with the oxide-component of the In 3d spectra, with the area contribution of In_2O_3 dropping significantly as In decreases. This change is more prominent than that of the Ga_2O_3 component of the Ga 2p spectra. In general, for the cleaned $In_xGa_{1-x}N$ gradient, a corresponding gradient in the surface chemistry is observed for all elements.

Following treatment with pH 6 L-arginine, an increase in the surface carbon, oxygen, and nitrogen are expected, in part because of the presence of the arginine carboxyl, amine, and

dx.doi.org/10.1021/am4015555 | ACS Appl. Mater. Interfaces 2013, 5, 7236−7243

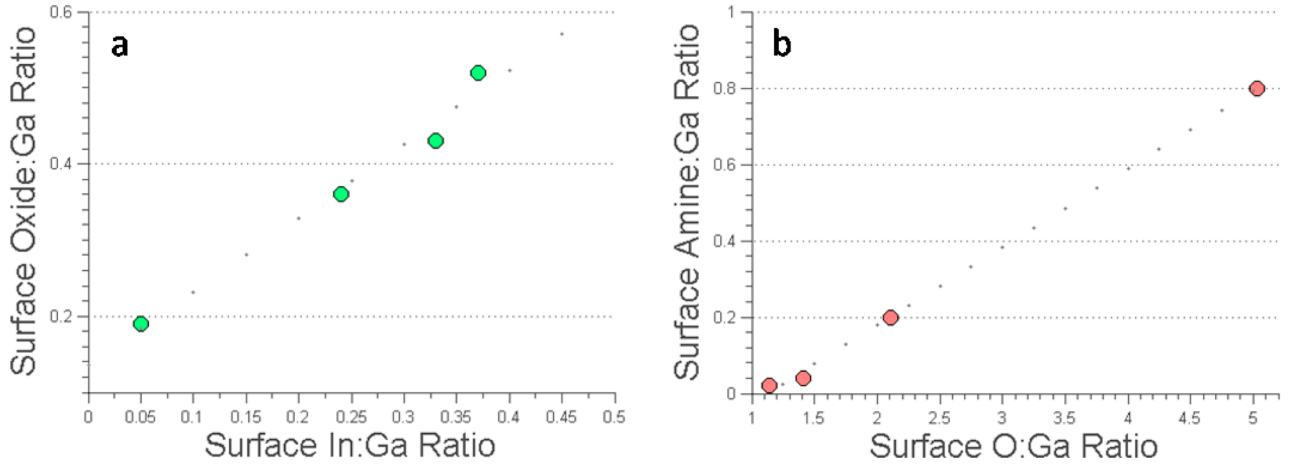

Figure 8. Graphical representation of the correlation between (a) surface oxide and In:Ga ratio on the clean surface (R^2 = 0.9758, p-value = 0.0122) and (b) surface-adsorbed amine and surface oxide following pH 6 arginine exposure (R^2 = 0.9987, p-value = 0.0013.).

guanidium groups. Again, a gradient from the high-In regions to the low-In regions is observed throughout the surface chemistry, with the surface oxygen displaying the expected drop as In decreases, and the quantity of surface carbon is higher for higher In:Ga. An increase in the relative surface presence of NH_2 and NH_3^+ groups is reported, and the trend in NH_2/NH_3^+:Ga values closely follows the trend in O:Ga. Figure 8 provides a graphical representation of this relationship. The linear correlation between surface oxide and the surface In:Ga ratio, seen in Figure 8a, is echoed by the observed linear correlation between surface-adsorbed amine and surface oxide following exposure to protonated arginine, seen in Figure 8b.

The data for pH 12 L-arginine are not displayed here due to the disappearance of the In and Ga signatures from all spectra. Representative Ga 2p and In 3d spectra are provided in the Supporting Information with the pH 6 spectra for comparison (see Figure S5 in the Supporting Information). As described above, the prominence of an amine signature in the N 1s spectrum (see Figure S4 in the Supporting Information) suggests that there is amino acid on the surface; however, the absence of In and Ga indicate that the surface coverage of L-arginine extends beyond the XPS penetration depth of ~3 nm. To confirm that signal disappearance was due to this multilayer (as opposed to sample damage or errors in preparation), we carefully rinsed samples with deionized water, dried them, and reintroduced them to the sample chamber. There is a re-emergence of the Ga and In signatures in these spectra (see the Supporting Information, Figure S6), indicating that the surface multilayer has been diminished. This supports the idea that deprotonating L-arginine diminishes the electrostatic repulsion between molecules, allowing a degree of accumulation that is otherwise prevented. The re-emergent Ga and In signatures are also stronger in the low-In regions of the substrate, supporting the observed trend in preferential adhesion of amino-acid to high-In regions. Thus, our chemical analysis of the substrate–arginine interface verifies differential adhesion of arginine across the compositional material gradient.

CONCLUSIONS

We present an $In_xGa_{1-x}N$ gradient platform with variable topographic, chemical, and optical properties dependent on the ratio of In:Ga. Adsorption of amino acid to this substrate is dependent on the underlying topography and chemistry, with an increase in adsorption as the surface presence of In increases. This is attributed to interactions between the surface oxide, which forms more readily in higher-In regions, and the positively charged amino acid. The reduction in electrostatic repulsion caused by deprotonation of the arginine α-amine group results in the formation of a multilayer of sufficient thickness to occlude the underlying substrate in chemical analysis via XPS. In the protonated state, distinct clusters of arginine form on the substrate, representing a balance between substrate-amino acid and amino acid-amino acid interactions. Amino acid adsorption increases with an increase in substrate In composition; thus, we confirm that surface gradients of biomolecules can be prepared by taking advantage of substrate gradients generated during initial material growth, and we propose that the use of recognition peptide sequences will allow for the construction of specific and continuous gradient interfaces without specialized functionalization processes.

ASSOCIATED CONTENT

Supporting Information

Additional characterization using PL, AFM, and XPS is presented. This material is available free of charge via the Internet at http://pubs.acs.org.

AUTHOR INFORMATION

Corresponding Author

*E-mail: ivanisevic@ncsu.edu. Phone: (919) 515-4683.

Present Address

[§]Affinergy, LLC, Morrisville, NC 27560

Author Contributions

The manuscript was written through contributions of all authors. All authors have given approval to the final version of the manuscript.

Notes

The authors declare no competing financial interest.

ACKNOWLEDGMENTS

We thank NC State University for start-up funds.

REFERENCES

(1) Ponce, F. A.; Bour, D. P. *Nature* **1997**, *386* (6623), 351–359.
(2) Chin, V. W. L.; Tansley, T. L.; Osotchan, T. *J. Appl. Phys.* **1994**, *75* (11), 7365–7372.

(3) Pearton, S. J.; Norton, D. P.; Ren, F. *Small* **2007**, *3* (7), 1144−1150.
(4) Chaniotakis, N.; Sofikiti, N. *Anal. Chim. Acta* **2008**, *615* (1), 1−9.
(5) Kuykendall, T.; Ulrich, P.; Aloni, S.; Yang, P. *Nat. Mater.* **2007**, *6* (12), 951−956.
(6) Gupta, S.; Elias, M.; Wen, X. J.; Shapiro, J.; Brillson, L.; Lu, W.; Lee, S. C. *Biosens. Bioelectron.* **2008**, *24* (4), 505−511.
(7) Jewett, S. A.; Makowski, M. S.; Andrews, B.; Manfra, M. J.; Ivanisevic, A. *Acta Biomater.* **2012**, *8* (2), 728−733.
(8) Chen, C. R.; Young, T. H. *Biomaterials* **2008**, *29* (11), 1573−1582.
(9) Estephan, E.; Saab, M. B.; Martin, M.; Larroque, C.; Cuisinier, F. J. G.; Briot, O.; Ruffenach, S.; Moret, M.; Gergely, C. *J. Peptide Sci.* **2011**, *17* (2), 143−147.
(10) Ivanisevic, A.; Yeh, J. Y.; Mawst, L.; Kuech, T. F.; Ellis, A. B. *Nature* **2001**, *409* (6819), 476−476.
(11) López-Gejo, J.; Arranz, A.; Navarro, A.; Palacio, C.; Munoz, E.; Orellana, G. *J. Am. Chem. Soc.* **2010**, *132* (6), 1746−1747.
(12) López-Gejo, J.; Navarro-Tobar, Á.; Arranz, A.; Palacio, C.; Muñoz, E.; Orellana, G. *ACS Appl. Mater. Interfaces* **2011**, *3* (10), 3846−3854.
(13) Cimalla, I.; Will, F.; Tonisch, K.; Niebelschutz, M.; Cimalla, V.; Lebedev, V.; Kittler, G.; Himmerlich, M.; Krischok, S.; Schaefer, J. A.; Gebinoga, M.; Schober, A.; Friedrich, T.; Ambacher, O. *Sens. Actuators, B* **2007**, *123* (2), 740−748.
(14) Yu, J. J.; Jha, S. K.; Xiao, L. D.; Liu, Q. J.; Wang, P.; Surya, C.; Yang, M. *Biosen. Bioelectron.* **2007**, *23* (4), 513−519.
(15) Steinhoff, G.; Baur, B.; Wrobel, G.; Ingebrandt, S.; Offenhausser, A.; Dadgar, A.; Krost, A.; Stutzmann, M.; Eickhoff, M. *Appl. Phys. Lett.* **2005**, *86* (3), 033901−033901.
(16) Stutzmann, M.; Garrido, J. A.; Eickhoff, M.; Brandt, M. S. *Phys. Status Solidi A* **2006**, *203* (14), 3424−3437.
(17) Kim, H.; Colavita, P. E.; Metz, K. M.; Nichols, B. M.; Sun, B.; Uhlrich, J.; Wang, X.; Kuech, T. F.; Hamers, R. J. *Langmuir* **2006**, *22* (19), 8121−8126.
(18) Stine, R.; Simpkins, B. S.; Mulvaney, S. P.; Whitman, L. J.; Tamanaha, C. R. *Appl. Surf. Sci.* **2010**, *256* (13), 4171−4175.
(19) Koepsel, J. T.; Murphy, W. L. *ChemBioChem* **2012**, *13* (12), 1717−1724.
(20) Chiu, C. S.; Lee, H. M.; Gwo, S. *Langmuir* **2010**, *26* (4), 2969−2974.
(21) Gray, D. S.; Tien, J.; Chen, C. S. *J. Biomed. Mater. Res., Part A* **2003**, *66A* (3), 605−614.
(22) Albert, J. N. L.; Baney, M. J.; Stafford, C. M.; Kelly, J. Y.; Epps, T. H. *ACS Nano* **2009**, *3* (12), 3977−3986.
(23) Higuchi, A.; Ling, Q.-D.; Chang, Y.; Hsu, S.-T.; Umezawa, A. *Chem. Rev.* **2013**, *113* (5), 3297−3328.
(24) Willett, R. L.; Baldwin, K. W.; West, K. W.; Pfeiffer, L. N. *Proc. Natl. Acad. Sci. U.S.A.* **2005**, *102* (22), 7817−7822.
(25) Whaley, S. R.; English, D. S.; Hu, E. L.; Barbara, P. F.; Belcher, A. M. *Nature* **2000**, *405* (6787), 665−668.
(26) Estephan, E.; Larroque, C.; Cloitre, T.; Cuisinier, F. J. G.; Gergely, C. *Proc. SPIE* **2008**, *6991*, 699121−699121.
(27) Bachmann, M.; Goede, K.; Beck-Sickinger, A. G.; Grundmann, M.; Irback, A.; Janke, W. *Angew. Chem., Int. Ed.* **2010**, *49* (49), 9530−9533.
(28) Bedair, S. M.; McIntosh, F. G.; Robert, J.; Piner, E.; Boutros, K.; ElMasry, N. A. *J. Cryst. Growth* **1997**, *178*, 32.
(29) Parker, C.; Roberts, J.; Bedair, S.; Reed, M.; Liu, S.; Elmasry, N.; Robins, L. *Appl. Phys. Lett.* **1999**, *75*, 2566.
(30) Wang, C. J.; Li, X.; Lin, B.; Shim, S.; Ming, G. L.; Levchenko, A. *Lab Chip* **2008**, *8* (2), 227−237.
(31) Weibel, D. B.; Whitesides, G. M. *Curr. Opin. Chem. Biol.* **2006**, *10* (6), 584−591.
(32) Dillmore, W. S.; Yousaf, M. N.; Mrksich, M. *Langmuir* **2004**, *20* (17), 7223−7231.
(33) Higashi, J.; Nakayama, Y.; Marchant, R. E.; Matsuda, T. *Langmuir* **1999**, *15* (6), 2080−2088.
(34) Park, S.; Yousaf, M. N. *Langmuir* **2008**, *24* (12), 6201−6207.
(35) César, M.; Ke, Y.; Ji, W.; Guo, H.; Mi, Z. *Appl. Phys. Lett.* **2011**, *98*, 202107−202109.
(36) Z. Chen, L. W. S., Shi, J. Y.; Wang, X. L.; Tang, C. L.; Gao, P. AFM Application in III-Nitride Materials and Devices. In *Atomic Force Microscopy−Imaging, Measuring, and Manipulating Surfaces at the Atomic Scale*; Bellitto, V., Ed.; InTech: Rijeka, Croatia, **2012**; pp 189−208.
(37) Heying, B.; Tarsa, E. J.; Elsass, C. R.; Fini, P.; DenBaars, S. P.; Speck, J. S. *J. Appl. Phys.* **1999**, *85*, 6470−6476.
(38) Jain, S. C.; Willander, M.; Narayan, J.; Van Overstraeten, R. *J. Appl. Phys.* **2000**, *87* (3), 965−1006.
(39) Nakamura, S.; Mukai, T.; Senoh, M. *Appl. Phys. Lett.* **1994**, *64* (13), 1687−1689.
(40) Krames, M. R.; Shchekin, O. B.; Mueller-Mach, R.; Mueller, G. O.; Zhou, L.; Harbers, G.; Craford, M. G. *J. Display Technol.* **2007**, *3* (2), 160−175.
(41) Procop, M. *J. Electron Spectrosc. Relat. Phenom.* **1992**, *59* (2), R1−R10.
(42) Makowski, M. S.; Zemlyanov, D. Y.; Ivanisevic, A. *Appl. Surf. Sci.* **2011**, *257* (10), 4625−4632.
(43) Hall, J. E.; Guyton, A. C. *Guyton and Hall Textbook of Medical Physiology*, 12th ed.; Saunders Elsevier: Philadelphia, PA, 2011; p 425.
(44) Keenan, T. M.; Folch, A. *Lab Chip* **2008**, *8* (1), 34−57.
(45) Goede, K.; Grundmann, M.; Holland-Nell, K.; Beck-Sickinger, A. G. *Langmuir* **2006**, *22* (19), 8104−8108.
(46) Dziecielewski, I.; Weyher, J. L.; Dzwolak, W. *Appl. Phys. Lett.* **2013**, *102* (4), 043704−043704.
(47) Butt, H. J.; Berger, R.; Bonaccurso, E.; Chen, Y.; Wang, J. *Adv. Colloid Interface Sci.* **2007**, *133* (2), 91−104.
(48) Rief, M.; Gautel, M.; Oesterhelt, F.; Fernandez, J. M.; Gaub, H. E. *Science* **1997**, *276* (5315), 1109−1112.